2014 IEEE International Conference on Robotics & Automation (ICRA)
Hong Kong Convention and Exhibition Center
May 31 - June 7, 2014. Hong Kong, China

Torque Estimation of Robot Joint with Harmonic Drive Transmission Using a Redundant Adaptive Robust Extended Kalman Filter

Zhiguo Shi and Guangjun Liu, *Senior Member, IEEE*

***Abstract*— A torque estimation method with adaptive robustness and optimality adjustment according to the load for modular and reconfigurable robot joint with harmonic drive transmission is proposed, on the basis of harmonic drive compliance model and redundant adaptive robust extended Kalman filter (RAREKF). The proposed approach can adapt torque estimation filtering optimality and robustness to the load variations by self-tuning the filtering gain and self-switching the filtering modes between optimal and robust. The redundant factor of RAREKF is designed as a function of the load to provide desirable tolerant capability to the modeling error and load-dependent filtering mode switching. The proposed joint torque estimation method has been experimentally studied in comparison with a commercial sensor, and the results have demonstrated the effectiveness of the proposed torque estimation technique.**

I. Introduction

Harmonic drives, invented in the 1950s [1], are widely used in robotic systems, due to their desirable features of near-zero backlash, compactness, light weight, high torque capacity, high gear ratio and coaxial assembly. These distinctive characteristics of harmonic drives vindicate their widespread applications, especially in electrically-driven robot manipulators. Joint torque feedback (JTF) has been widely recognized to improve the performance of robot control in the robotics community [2], [3]. The JTF is generally used in motion control of robot manipulators to suppress the effect of load torques [4]. In addition, joint torque sensors can considerably ease the necessity to model the link dynamics. JTF can be used in the dynamic control of robots without the need of computing the robot inverse dynamics. In addition, joint torque sensing is necessary for collision detection and reaction.

Measurement or estimation of the torque transmitted by the harmonic drive transmission is required for the implementation of JTF control methods. Conventionally, to implement such control strategies, the robot is equipped with joint torque sensors or a multi-axis force/torque (F/T) sensor. When using F/T sensor at the robot wrist, the estimation of joint torques requires additional calculations, and the results may be affected by computation delays and model errors [5]. There are several techniques of direct joint torque sensing, including joint torque sensors based on elastic elements that are placed in the output transmission line of each joint of the robot [6], [7].

In [8], a linear encoder is used to measure the torsional deformation of the additional elastic body of a joint torque sensor. As measurement accuracy is in inverse proportion to sensor stiffness, low sensor stiffness is desirable in order to achieve high measurement resolution, which leads to complicated joint dynamics. Another joint torque sensing technique is based on the method proposed by Hashimoto et al. [9]. Joint torque sensing is achieved by mounting strain gages directly on the harmonic drive, which is usually referred to as built-in torque sensing for harmonic drives [9], [10], [11]. The torsional compliance of harmonic drives lends itself to torque sensing, but the measurement signals contain substantial ripples. It is difficult to extract the applied torque from the signals with ripples [12].

Torque estimation using harmonic drive compliance model provides an effective way of torque estimation for robot joints with harmonic drive and accurate link-side position measurement [13]. The joint torque estimation technique uses measurements of both the link-side and motor shaft positions along with a proposed harmonic derive model to realize stiff and sensitive torque estimation, obtaining joint torque with minimal mechanical modifications. However, a low-pass filter is used in [13] to filter the output of the harmonic drive model, which presents a simple and convenient way to resist high frequency noises, but the influence of the load variation is not taken into consideration and the estimation response speed is limited by the filter bandwidth.

In [10], to minimize sensing inaccuracy, four rosette strain gauges are used with accurate positioning on the flexspline. To cancel the torque ripples, the oscillation observed on the measured torque and caused mainly by gear teeth meshing, standard Kalman filter estimation is used. With on-line implementation of a Kalman filter, it has been demonstrated with experiments that this method is a fast and accurate way to filter torque ripples and torque due to misalignment.

Kalman optimal filtering technique is commonly used in torque estimation algorithms. However, the filter gain is optimal and cannot be self-adjusted in the standard Kalman filter algorithm, and the external environment is only reflected by the pre-set measurement noise variance, which makes it difficult to adapt to changes in the actual external disturbance and respond timely. Disturbances are taken into account in real time according to the actual measurement in the robust filtering algorithm [14], [15], where the online estimation of

This work is supported in part by the Natural Sciences and Engineering Research Council (NSERC) of Canada and in part by the Canada Research Chair program. The first author is also supported by NSFC under Grant No. 60903067 and Beijing Natural Science Foundation under Grant No. 4122049.

The authors are with the Department of Aerospace Engineering, Ryerson University, 350 Victoria Street, Toronto, Ontario, Canada M5B 2K3. Z. Shi is a Visiting Professor from the School of Computer and Communication Engineering, University of Science and Technology Beijing, 100083, China. G. Liu is the corresponding author. Email:gjliu@ryerson.ca.

the noise variance [14] and resetting recursive prediction error variance [15] are incorporated to adjust the filter gain online. That improves the adaptability of the filters to disturbances and ensures the robustness of the algorithm.

However, as robustness conflicts with optimality, robust performance improvement is often accompanied by performance loss. In case that disturbance does not always exist in the filtering process, strong robustness is not required all the time, and it causes excessive loss of optimality. In [15], an adaptive robust extended Kalman filter (AREKF) is proposed to switch the working mode of the filter between robust and optimal, adaptively adjusting the filtering gain with the functions of automatic determination and switching. However, nonlinear modeling error in the state and measurement models may cause failure in the switching function of judgment mechanisms of AREKF, making the AREKF always work in robust filtering mode. To solve this problem, redundant parameters are introduced into the AREKF, and redundant adaptive robust extended Kalman filter (RAREKF) [16] is used to make the switching function work stably within the range of a certain redundancy and switch when necessary.

In this paper, a joint torque estimation method is developed based on a harmonic drive model and a redundant adaptive robust extended Kalman filter, which can provide desirable tolerant capability to the modeling error and dynamic adjustment of the balance between optimality and robustness according to the load variation. The proposed method consists of a modeling part and a filtering part. The modeling part models the harmonic drive compliance on the basis of three readings: link-side absolute encoder readings, motor-side encoder readings and motor current readings. The output of the modeling part provides the input to the filtering part consisting of a redundant adaptive robust extended Kalman filter. The proposed method has been studied experimentally, and the experimental results have demonstrated the effectiveness of the proposed joint torque estimation method.

The rest of the paper is organized into five sections as follows: the overall torque estimation structure is presented in Section 2. The modeling of harmonic drive torque system and an adaptive torque estimation algorithm are presented in Section 3 and Section 4, respectively. Experimental results are given and discussed in Section 5, and concluding remarks are in Section 6.

II. Overall Structure of Torque Estimation

The overall structure of the proposed torque estimation method is as shown in Fig. 1. The redundant adaptive robust extended Kalman filter (RAREKF) is introduced in the filtering part to deal with modeling error and disturbances, and more importantly, to balance optimality and robustness according to the load variation.

As a result of load variation, the torque is changing, robustness is needed in order to make the estimation respond rapidly. However, strong robustness is not required all the time, which will cause excessive loss of optimality. RAREKF provides adaptively switching the filtering state between the optimality and robustness according to the load change, which can effectively guarantee the accuracy and fast response. In addition, RAREKF make the switching function work stably within the range of a certain redundancy and switch when necessary.

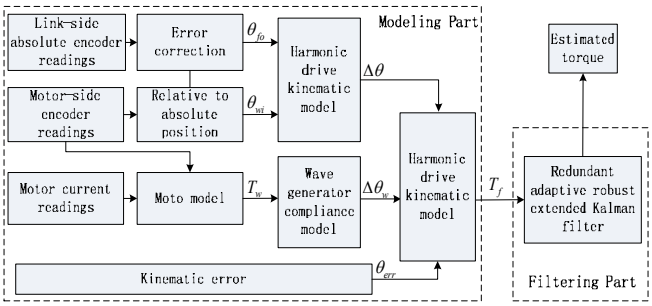

Figure 1. Overall structure of the torque estimation.

III. Modeling of Harmonic Drive Torque

A harmonic drive consists of three main components as shown in Fig. 2.

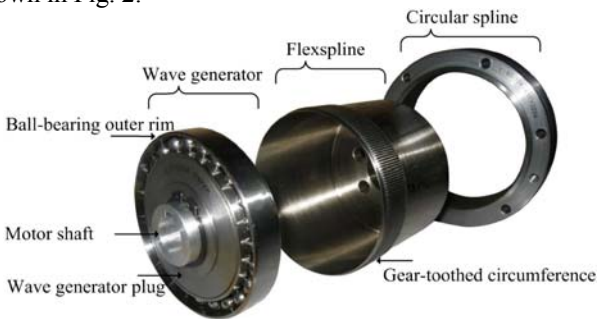

Figure 2. Three components of a harmonic drive.

Typically the wave generator (WG) is connected to the motor shaft, the circular spline (CS) is connected to the joint housing, and the flexspline (FS) is sandwiched in between (CS and WG) and connected to the joint output. The WG consists of an elliptical disk (rigid elliptical inner-race), called wave generator plug, and an outer ball bearing.

The wave generator plug is inserted into the bearing, thereby giving the bearing an elliptical shape as well. The FS fits tightly over WG; when the WG plug is rotated, the FS deforms and molds into the shape of the rotating ellipse but does not rotate with WG.

The modeling of harmonic drive kinematic can be seen in our lab's previous work [13]. $\Delta\theta$ is the total torsional angle of the harmonic drive, $\Delta\theta_f$ is the torsional angle of the flexspline , $\Delta\theta_w$ is wave generator torsional angle, θ_{err} is the kinematic error. From [13],

$$\Delta\theta = \Delta\theta_f + \frac{\Delta\theta_w}{N} + \theta_{err} \quad (1)$$

A typical harmonic drive stiffness curve is shown in Fig. 3, which features increasing stiffness with displacement and hysteresis behavior. The total harmonic drive torsional deformation comprises deformation of both the flexspline and the wave generator. A model of the compliance of harmonic drive component is presented in the following.

Based on the curve shown in Fig. 3 and experimental observation, the harmonic drive torsional deformation is largely contributed by the flexspline torsional compliance. The flexspline torsional compliance is described in [17], where $\Delta\theta_f$ is approximated by a piecewise linear function of the output torque.

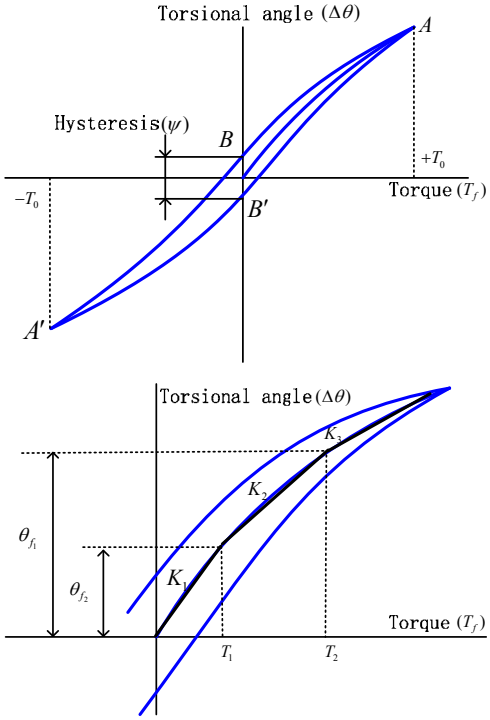

Figure 3. Typical stiffness and hysteresis curve of a harmonic drive.

$$\Delta\theta_f = \begin{cases} \frac{T_f}{K_1}, & T_f \le T_1 \\ \frac{T_1}{K_1} + \frac{(T_f - T_1)}{K_2}, & T_1 < T_f < T_2 \\ \frac{T_1}{K_1} + \frac{(T_2 - T_1)}{K_2} + \frac{(T_f - T_2)}{K_3}, & T_f \ge T_2 \end{cases} \quad (2)$$

where K_1, K_2, K_3, T_1, and T_2 are given by the manufacture. The slope of the curve shown in Fig. 3 determines the harmonic drive stiffness. For simplicity, the curve is approximated by three straight-line segments with stiffness of K_1, K_2, and K_3. Stiffness K_1 applies for flexspline torque of 0 to T_1. Stiffness K_2 applies for flexspline ranging from T_1 to T_2. Stiffness K_3 applies for flexspline torque greater than T_2.

It is well known that harmonic drives suffer from both nonlinear torsional compliance and hysteresis behavior. We assume that hysteresis is caused by the compliance of the wave generator and the harmonic drive friction. When the wave generator's torque (torque applied by the motor) is within harmonic drive's starting torque, the harmonic drive's output torque will not change.

Therefore, the harmonic drive torsional deformation can be from $-\Psi/2$ to $\Psi/2$ at zero torque output. In our lab's previous work [13], to replicate the hysteresis shape of this stiffness curve, the wave generator local elastic coefficient is model as

$$K_w = K_{w0} e^{C_w |T_w|} \quad (3)$$

where K_{w0} and C_w are constants to be determined. The wave generator torsional angle can be calculated using the following relation.

$$\Delta\theta_w = \int_0^{T_w} \frac{dT_w}{K_w} \quad (4)$$

Substituting Eq. (3) into Eq. (4), we obtain

$$\Delta\theta_w = \frac{sign(T_w)}{C_w K_{w0}} (1 - e^{-C_w |T_w|}) \quad (5)$$

The total torsional deformation of the harmonic drive is measured using both link-side and motor-side encoders. The wave generator torque T_w is approximated by the motor torque command.

Combining (5) with (1) yields

$$\Delta\theta_f = \Delta\theta - \frac{sign(T_w)}{C_w N K_{w0}} \left(1 - e^{-C_w |T_w|}\right) - \theta_{err} \quad (6)$$

Using the inverse of Eq. (2), the output of harmonic drive compliance model can be presented as

$$T_f = \begin{cases} K_1 \Delta\theta_f, & \Delta\theta_f \le \theta_{f_1} \\ T_1 + K_2(\Delta\theta_f - \theta_{f_1}), & \theta_{f_1} < \Delta\theta_f < \theta_{f_2} \\ T_2 + K_3(\Delta\theta_f - \theta_{f_2}), & \Delta\theta_f \ge \theta_{f_2} \end{cases} \quad (7)$$

where $\theta_{f_1} = T_1/K_1$ and $\theta_{f_2} = T_1/K_1 + (T_2 - T_1)/K_2$.

IV. THE REDUNDANT ADAPTIVE ROBUST EXTENDED KALMAN FILTER

The estimation result calculated from model cannot be used directly for the implementation of the robotic joint control because of the inevitable noise, which necessitates the utilization of the filtering algorithm. Due to the unknown change of load, robust filtering is required in order to have a quick response to the influence of the torque from load variation. Considering that the estimation precision is sacrificed in the robust filtering, adaptive robust filtering is adopted because it can restrain the excessive sacrifice by introducing self-switching of the filtering modes between optimal and robust.

However, for the joint torque estimation problem concerned in this paper, the model cannot be completely accurate and has modeling error varying with load. To handle the effect of the inner modeling errors to the estimation result, a redundant adaptive robust extended Kalman filtering algorithm [16] is applied. The method has a redundant factor which can help reduce the impact of the modeling error to the precision of the estimation result. Noticing that the modeling errors are dependent on the joint load, the redundancy factor is designed, which is a function of the current load such that the error-tolerant capability of the filter can be adjusted according to the load. In this way, the filtering mode can be switched between the robustness and optimality when the load-dependent modeling error exists.

Considering that the torque change is unknown, we write the filtering model as

$$X(k) = f(k, X(k-1)) + w(k) \quad (8)$$

$$Y(k) = H(k)X(k) + v(k) \quad (9)$$

where $k \in N$, the state variable $X \in R^n$ represents T_f in Eq. (7). $X(k)$ is the state of the system on the time step k and $Y(k)$ is the measurement on the time step k, while n and m is the spatial dimensions. The measurement $Y \in R^m$ is the calculation result from the torque model. The measurement matrix H and the system function $f(x)$ are continuously differentiable. According to the harmonic drive compliance model described by Eq. (7), there are $H=I$ and $f(k, X(k-1)) = X(k-1)$. w and v are uncorrelated zero-mean Gaussian white noise, W and V are their covariance matrix, respectively. The robust filtering algorithm based on the gain adjustment will be unified in the following algorithm.

1) State Prediction: The one-step state prediction and its covariance matrix are

$$\hat{X}(k|k-1) = f(k, \hat{X}(k-1|k-1)) \quad (10)$$

$$P(k|k-1) = F(k-1)P(k-1|k-1)F^T(k-1) + W(k-1) \quad (11)$$

where $F = \partial f(X)/\partial X|_{X=\hat{X}}$ is the Jacobian matrix of $f(X)$.

2) Gain Adjustment: The covariance matrix of prediction error is modified by

$$\sum(k|k-1) = S(P(k|k-1)) \quad (12)$$

where S is a gain scheduling operator.

3) Measurement Innovation: The innovation from measurements and its covariance matrix are

$$\tilde{Y}(\mathrm{k}) = Y(k) - H(k-1)\hat{X}(k|k-1) \quad (13)$$

$$P_Y(k) = H(k-1)\sum(k|k-1)H^T(k-1) + V(k) \quad (14)$$

4) Estimation Update: The filtering gain and the estimation of state with its covariance matrix are

$$K(k) = \sum(k|k-1)H^T(k)P_Y^{-1}(k) \quad (15)$$

$$\hat{X}(k|k) = \hat{X}(k|k-1) + K(k)\tilde{Y}(k) \quad (16)$$

$$P(k|k) = (\sum{}^{-1}(k|k-1) + H^T(k)V^{-1}(k)H(k))^{-1} \quad (17)$$

When S is an identity operator, the algorithm is equivalent to the standard extended Kalman filtering algorithm. However in a robust extended Kalman filtering algorithm, S is often derived from a robustness index.

The indicator design of a typical linear $H\infty$ robust filtering algorithm is to ensure the stability of filtering in the linearization error [14]. The gain scheduling operator is often taken as:

$$\sum(k|k-1) = (P^{-1}(k|k-1) - \gamma^{-2}L^T(k)L(k))^{-1} \quad (18)$$

where $L(k) \in R^n$ is an adjustable matrix. The attenuation factor γ is defined as the supremum of the ratio of the amplitude of estimation error and the summation of all the other errors. These errors include the measurement noises, the external disturbance, and the modeling error. The balance of robustness and optimality is guaranteed by tuning the attenuation factor. The robustness of filtering algorithm is reduced with the increase of γ, the robustness of filtering algorithm is reduced. When $\gamma = \infty$, the robust filtering is degenerated to the extended Kalman filter.

The attenuation factor is user-defined and has drawback. Because once γ is given, the algorithm will work in robust filtering mode, and may not achieve filtering optimality. For this reason, the adaptive robust extended Kalman filtering (AREKF) algorithm is provided with an adaptive switching mechanism of S to make the filter adaptive. In the AREKF [15], the gain scheduling operator S in Eq. (12) is determined by $P(k|k-1)$ and

$$\sum(\mathrm{k|k-1}) = \begin{cases} (P^{-1}(k|k-1) - \gamma^{-2}L^T(k)L(k))^{-1}, & \bar{P}_Y(k) > \alpha P_Y(k) \\ P(k|k-1), & otherwise \end{cases} \quad (19)$$

The algorithm will be in the robust filtering mode if the measurement error variance $P_Y(k)$ is less than the value of $\bar{P}_Y(k)$. α is the redundancy factor, defined in (23), and $\bar{P}_Y(k)$ is defined as

$$\bar{P}_Y(k) = \begin{cases} \tilde{Y}(k)\tilde{Y}^T(k), & k = 0 \\ \frac{\rho P_Y(k-1) + \tilde{Y}(k)\tilde{Y}^T(k)}{\rho+1}, & k > 0 \end{cases} \quad (20)$$

where ρ is a forgetting factor. In order to satisfy the filtering stability condition, as given in [16]

$$L(k) = \gamma(P^{-1}(k|k-1) - \bar{\varepsilon}_{max}^{-2}I)^{1/2} \quad (21)$$

and the compensation factor $\bar{\varepsilon}_{max}^{-2}I$ in $L(k)$ satisfies

$$\bar{\varepsilon}_{max}^{-2}I \le \bar{\sum}^{-1}(k|k-1) \quad (22)$$

The AREKF algorithm is defined by Eqs. (19), (20), (21) and (22) together with (10) - (17).

The objective of AREKF is to achieve adaptive real-time switching of the filtering mode based on the innovation rate. However, the switching mechanism cannot work properly because of the existence of modeling error. That makes $\bar{P}_Y(k) > \alpha P_Y(k)$ always hold when $\alpha = 1$. So in the actual process, Eq. (19) will be identical to Eq. (18).

The robust filtering status will not be triggered by small error, which is only needed to be detected when the modeling error exceeds a threshold. Thus, redundancy is required to be introduced to recover the switching function of Eq. (19), that is $\alpha > 1$. In addition, the compensation function $\bar{\varepsilon}_{max}^{-2}I$ is not explicitly expressed and cannot be adjusted flexibly, although it avoids the difficulty of determining the fading factor.

Therefore, we introduce the redundancy factor and the compensation function in AREKF and establish a redundant AREKF algorithm for application on the torque estimation.

As confirmed by experiments, the modeling error depends on the load of the joint. The modeling error increases with the torque load, so that the redundant factor needs also to be increased to avoid the excessive loss of filtering optimality. Hence, denoting ω as the torque load, the redundant factor is designed as

$$\alpha = \begin{cases} k\omega^2, & k\omega^2 < 1 \\ 1, & otherwise \end{cases} \quad (23)$$

And the compensation function is defined as follows:

$$\bar{\varepsilon}_{max}^{-2}I = f_\alpha^{-1}(k)P^{-1}(k|k-1) \quad (24)$$

where the compensation factor is:

$$f_\alpha(k) = \alpha^{-1}diag\left[\frac{\bar{P}_Y(k)}{P_Y(k)}\right] \quad (25)$$

which can guarantee the filtering stability in the case that the redundant factor $\alpha \neq 1$ [18].

Taking Eqs. (20) - (25) into Eq. (12) and replacing Eq. (12) with Eq. (19), the RAREKF for torque estimation can be fully represented by Eqs. (10) - (17).

The redundant factor in RAREKF is utilized to enhance the capability of modeling error tolerance. Due to the existence of the redundant factor, the filtering mode switching function may provide a tunable judgment threshold. Typically, we let the threshold be the upper bound of the modeling error, which means that the filter switches to the robust filtering mode only if there is an external disturbance beyond the modeling error. That can help decrease the unnecessary loss of optimality caused by the modeling error. For this reason, the switching in RAREKF between optimal and robust filtering becomes much more effective and that leads to a reasonable balance between estimation precision and fast-following capability.

V. Experimental Results

Experiments have been conducted to investigate the effectiveness of the proposed approach, examining

particularly the issues of optimality and robustness, the difference between the estimated torque and torque sensor. Three different filtering algorithms have been implemented for comparison.

The harmonic drive of the test joint is driven by a brushed DC motor from Maxon, which is capable of delivering up to 0.191 *Nm*. The Maxon DC motor is coupled with a harmonic drive system model SHD-17-1002SH, with gear ratio of 100:1, and rated torque of 16 *Nm* from harmonic drive AG. The DC motor is instrumented with an optical incremental encoder with 4096 counts/rev to measure the rotor angular displacement.

The efficiency of the proposed torque estimation method is verified by comparing the estimated joint torque to the torque measurement from the ATI F/T sensor mounted on the output of the test joint.

A. Experiment on the Test Joint

The test joint setup is as shown in Fig. 4, which integrates a DC motor with incremental encoder, harmonic drive, link-side absolute encoder and an ATI F/T sensor. The correctness of the modeling part and the filtering results are verified with this experimental setup.

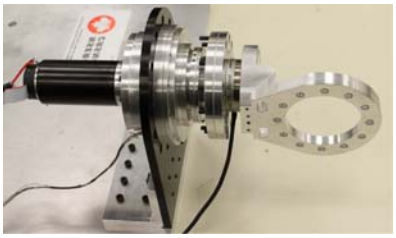

Figure 4. Joint with torque sensor.

The test joint is rotated 180^{o} in 80 seconds. Without additional load, the working mode of the filtering algorithm is in optimal to achieve more accurate estimation result. The estimated torque is compared to the torque sensor output in Fig. 5.

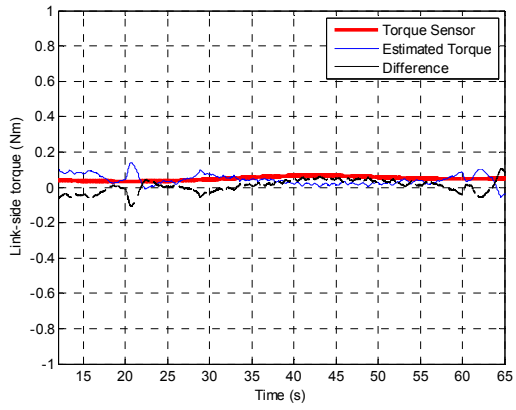

Figure 5. Experiment results of test joint without link-joint.

The curve of torque sensor in Fig. 5 is quickly followed by the estimated torque after a transient period. The difference between the estimated torque and sensor output is lower than 0.1 *Nm*.

B. Experiment with Link-joint Without External Force

In a general working state, the test joint is deployed with a link-joint, as normally for a robotic arm. A complete set of experiment system is set up as shown in Fig. 6 to verify the proposed torque estimation method.

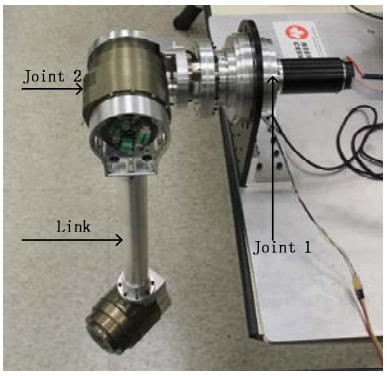

Figure 6. The experiment setup with link-joint.

In this experiment, the test joint is controlled to rotate with a desired trajectory: the initial position of the link-joint is in the vertical position, then the joint slowly rotates to the horizontal position in the clockwise direction. The load of the test joint will change gradually with its motion.

When the link-joint moves to the designated location, it will stop and maintain the location. In this process, the load of the test joint is gradually increasing, and reaches the maximum value when it stops. The difference between the estimated torque and torque sensor is presented in Fig. 7.

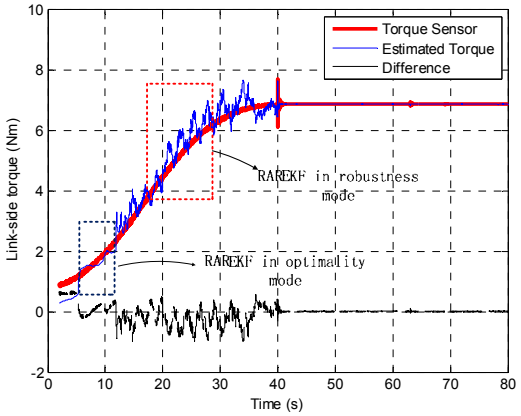

Figure 7. Experiment results with link-joint but no external force.

It can be seen that the RAREKF is in optimal mode at the beginning. The load increases with the link-joint rotation, and the working mode of RAREKF is gradually transiting to the robust mode. When the link-joint stops at the designated location, the torque is fixed. The difference between estimated torque and estimated torque is relatively high in the stage of RAREKF switching from optimality to robustness, but the error of the estimated torque is acceptable overall.

The working mode switching between optimal and robust according to the load variation is necessary. In the optimal mode, the torque estimation can effectively suppress the noises, but responds slowly to the load variation. In the robust

mode, the torque estimation can respond quickly to the load variation, with reduced effectiveness in noise suppression.

C. Experiment with External Force

Sudden external force is added to the previous experiment. The moving links and joints attached to the base joint introduce only gradual load change. To introduce fast torque changes, external torque is applied manually in both directions. The response of the proposed torque estimation method to sudden changes was verified by adding external force. The experimental procedure is almost the same with the previous experiment. The difference between the estimated torque and torque sensor is presented in Fig. 8. The details of the experimental result with sudden external force disturbance, as indicated in Fig. 8, are shown in Fig. 9.

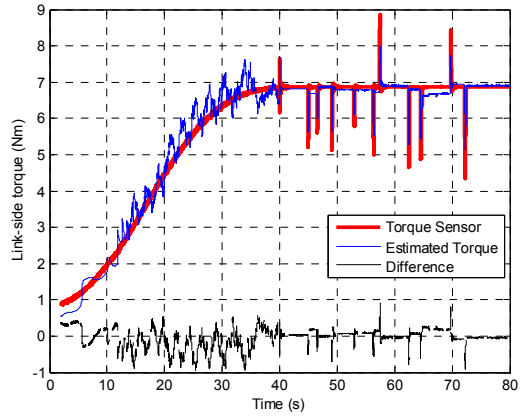

Figure 8. Experiment results of link-joint with external force.

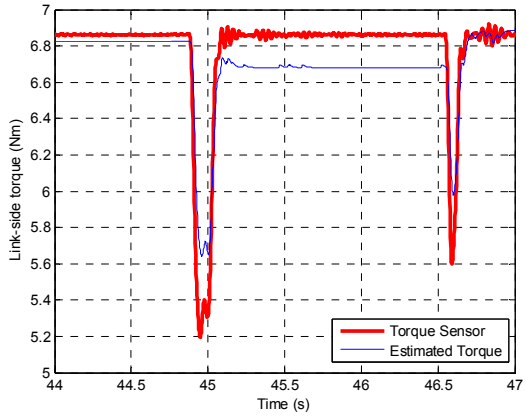

Figure 9. Zoomed view of the portion indicated in Fig. 8.

VI. Conclusion

The proposed torque estimation method provides desirable tolerant capability to the modeling error and dynamic balance of optimality and robustness according to the load variation. The effectiveness of the redundant adaptive robust extended Kalman filter for joint torque estimation has been demonstrated with experimental results.

In practice, the change rate of the filtering gain can be manually pre-set to get the better torque estimation performance and better noise resistance and external force response, according to the requirements of the systems. The future work will focus on the estimation optimization, as well as compensating the effect of the frictions.

Acknowledgment

The authors would like to thank Dr. Saleh Ahmad for the help on the experimental setup and Dr. Yuankai Li for insightful discussions on the RAREKF algorithm.

References

[1] C. W. Musser, "Strain wave gearing," Patent US 2 906 143, [Online]. Available: http://www.google.com/patents?vid=2906143. 1955.

[2] F. Aghili, M. Buehler, and J. M. Hollerbach, "Motion control systems with h-infinity positive joint torque feedback," IEEE Trans. on Control System Technology, vol. 9, no. 5, pp. 685–695, 2001.

[3] G. Liu, S. Abdul, and A. Goldenberg, "Distributed modular and reconfigurable robot control with torque sensing," in Proc. IEEE Int. Conf. on Mechatronics and Automation, pp. 384–389. 2006.

[4] F. Aghili, J. Hollerbach, and M. Buehler, "A modular and high-precision motion control system with an integrated motor," IEEE/ASME Trans. on Mechatronics, vol. 12, no. 3, pp. 317–329, 2007.

[5] M. Randazzo, M. Fumagalli, F. Nori, L. Natale, G. Metta, and G. Sandini, "A comparison between joint level torque sensing and proximal F/T sensor torque estimation: implementation on the icub," in Proc. IEEE/RSJ Int. Conf. on Intelligent Robots and Systems, pp. 4161–4167, 2011.

[6] D. Vischer and O. Khatib, "Design and development of high-performance torque-controlled joints," IEEE Trans. on Robotics and Automation vol. 11, no. 4, pp. 537–544, 1995.

[7] D. Tsetserukou, R. Tadakuma, H. Kajimoto, and S. Tachi, "Optical torque sensors for implementation of local impedance control of the arm of humanoid robot," In Proc. IEEE Int. Conf. on Robotics and Automation, pp. 1674–1679. 2006.

[8] T. Kawakami, K. Ayusawa, H. Kaminaga, and Y. Nakamura, "High-fidelity joint drive system by torque feedback control using high precision linear encoder," In Proc. IEEE Int. Conf. on Robotics and Automation, pp. 3904–3909, 2010.

[9] M. Hashimoto, Y. Kiyosawa, and R. Paul, "A torque sensing technique for robots with harmonic drives," IEEE Trans. on Robotics and Automation vol. 9, no. 1, pp. 108–116, 1993.

[10] H. Taghirad and P. Belanger, "Torque ripple and misalignment torque compensation for the built-in torque sensor of harmonic drive systems," IEEE Trans. on Instrumentation and Measurement. vol. 47, no. 1. pp. 309-315, 1998.

[11] I. Godler, M. Horiuchi, M. Hashimoto, and T. Ninomiya, "Accuracy improvement of built-in torque sensing for harmonic drives," IEEE/ASME Trans. on Mechatronics. vol. 5, no. 4, pp. 360–366, 2000.

[12] J. Sensinger and R. Weir, "Improved torque fidelity in harmonic drive sensors through the union of two existing strategies," IEEE/ASME Trans. on Mechatronics. vol. 11, no. 4, pp. 457–461, 2006.

[13] H. Zhang, S. Ahmad, and G. Liu, "Torque estimation of robot joint with harmonic drive transmission," In Proc. IEEE International Conference on Robotics and Automation, Karlsruhe, Germany, pp. 3019-3024, 2013.

[14] J. Seo, M.J. Yu, C.G. Park, and J.G. Lee, "An extended robust H∞ filter for nonlinear constrained uncertain systems," IEEE Transactions on Signal Processing. vol. 54, no. 11. pp. 4471-4475, 2006.

[15] K. Xiong, H. Zhang, and L. Liu, "Adaptive robust extended Kalman filter for nonlinear stochastic systems," IET Control Theory and Applications, vol. 2, no. 3, pp. 248-250, 2008.

[16] Y.K. Li, Z.L. Jing, and S.Q. Hu, "Redundant adaptive robust tracking of active satellite and error evaluation," IET Control Theory and Application, vol. 4, no. 11, 2010. pp. 2539-2553.

[17] Harmonic Drive Technologies. Ultra-flat component sets and gearheads. [Online]. http://www.harmonicdrive.net/ support/catalogs/. 2012.

[18] R. Knorad, G. Stefan, and Y. Engin, "Stochastic stability of the discrete-time extended Kalman filter," IEEE Transactions on Automatic Control, vol. 44, no. 4, pp. 714-728, 1999.